Ecological Complexity 6 (2009) 272–277

Contents lists available at ScienceDirect

Ecological Complexity

journal homepage: www.elsevier.com/locate/ecocom

Graph theory defining non-local dependency of rainfall in Northeast Brazil

C.N. de Santana [a,*], A.S. Fontes [b], M.A. dos S. Cidreira [b], R.B. Almeida [b], A.P. González [c], R.F.S. Andrade [d], J.G.V. Miranda [d]

[a] Universidade Estadual de Feira de Santana, Feira de Santana, Brazil
[b] Escola Politécnica da Universidade Federal da Bahia, Salvador, Brazil
[c] Universidad de A Coruña, La Coruña, Spain
[d] Instituto de Física, Universidade Federal da Bahia, Salvador, Brazil

ARTICLE INFO

Article history:
Available online 16 June 2009

Keywords:
Rainfall records
Pearson correlation
Power law dependence

ABSTRACT

This work shows that graph theory provides a framework to quantify the behavior of the time-correlation function among precipitation records within a given region. The method amounts to consider each station, where one data series was recorded, as a vertex in the graph. An edge, characterized by its geodesic distance d, is inserted between any pair of nodes, for which the Pearson correlation coefficient R, calculated from the corresponding series, is larger than a threshold value R_{th}. Then, the dependence between $N(\varepsilon)$, the total number of Pearson-correlated pairs of stations with geodesic distance $d \leq \varepsilon$, is evaluated as a function of ε. Results are presented for a set of spatially distributed pluviometric stations in Northeast Brazil. The reliability of the proposed procedure is tested in a two-fold way: First, values of $N(\varepsilon)$ are evaluated for graphs built up by sets of regular and random distributions of nodes within the actual region where the data is collected. Next, an investigation of the influence of the choice for R_{th} on the results is performed. The results lead to the identification of a power law $N(\varepsilon) \sim \varepsilon^{\alpha}$ for all time periods and regions that have been investigated, suggesting the presence of a robust non-metric fractal behavior. The value of α is found to depend both on seasonal and intrinsic features of the region rainfall distribution, but rather weakly on the value of R_{th}. The comparison of the results shows that, in contrast with the values obtained from Hurst exponent analysis, the values of α are related to the uniformity of Pearson correlation within the considered region, not with persistence of the signal.

© 2009 Elsevier B.V. All rights reserved.

1. Introduction

Rainfall events result from the interplay of several physical phenomena, most of which can be individually and adequately described by the basic laws of mechanics and thermodynamics. Despite the knowledge of the basic phenomena, the accurate description of an actual rainfall occurrence is still a rather complex issue, as this requires the assembling a huge number of individual events, for which we ought to know the proper initial and boundary conditions. In the last decades, a huge progress was achieved in both weather forecast and description of climate evolution. It results from several improvements in meteorological measurements and large-scale computing facilities, what makes it possible to run precise algorithms with accurate boundary conditions. The progress includes sophisticated analyses of recorded and simulated data, like spatial and temporal statistical correlations, scaling properties, topological properties of spatial event distribution, and so on. Finally, it also allows for an improved interpretation of past recorded data.

The investigation of historical rainfall records now includes several mathematical methods to detect spatial and temporal statistical scale invariance (Lovejoy and Mandelbrot, 1985; Lovejoy and Schertzer, 1991; Rubalcaba, 1997). This is a ubiquitous property found in a large number of natural systems that are characterized by a large number of degrees of freedom interacting in a complex nonlinear way (Koscielny-Bunde et al., 1998; Mandelbrot and Wallis, 1969; Mandelbrot, 1982; Turcotte, 1992).

In this work, we use concepts of graph theory to analyze spatial patterns in time-correlation function among rain events, using recorded data from a set of stations in Northeast Brazil. In previous contributions (Andrade et al., 1998; Miranda and Andrade, 1999; Miranda et al., 2004), we investigated properties of rain events in this region with concepts of statistical scale invariance within the data, which can be expressed in terms of temporal and spatial Hurst exponents. The method we use herein is similar to that proposed for the analysis of brain activity signals (Eguiluz et al., 2005). Within this approach, non-local spatial dependence is estimated by evaluating the Pearson coefficient between time series of pairs of stations.

* *Corresponding author.*
E-mail address: charles.santana@gmail.com (C.N. de Santana).

1476-945X/$ – see front matter © 2009 Elsevier B.V. All rights reserved.
doi:10.1016/j.ecocom.2009.05.011

As we will show later on, the main results of this work refer to a very clear scaling behavior of the distribution of the number of Pearson-correlated pairs of stations (i,j) with respect to the geodesic distance $d(i,j)$ (henceforth referred to as distance) between the stations (i,j) over the earth surface. The value of the power law exponent allows us to quantify the correlation magnitude. This way, we can identify sub-regions within Northeast Brazil that are subject to the same or distinct rainfall regimes. These results corroborate early findings based on Hurst exponent analyses.

This work is organized as follows: Section 2 reviews the most relevant features of the pluviometric regimes in Northeast Brazil and describes the data sets used in our study. Section 3 presents the very basic concepts of graph theory and the method used for graph construction based on the evaluation of the spatial correlation. Results are discussed in Section 4, while Section 5 closes the paper with a comparison of our results with those obtained by other approaches.

2. Data sets and climate in Northeast Brazil

Northeast Brazil is one of the largest regions of the world where semi-arid climatic condition prevails (Hastenrath et al., 1987; Nimer, 1989). The region extends over more than 1.540.000 km^2, from which some 512.000 km^2 at its south most part corresponds to the state of Bahia. Many global circulation systems influence the climate of the region, from which the most important are (Hastenrath, 1984; Chaves and Cavalcanti, 2001):

(a) The seasonal displacement of the of the inter-tropical convergence zone, which affects mostly the northern part of the region;
(b) The rather stable high-pressure zone in the center of Brazil during winter, which restricts the humid season of the inland to the late spring, summer and early autumn;
(c) The constant flow of sea wind in the humid east coast region;
(d) The influence, on the state of Bahia, of the low-pressure humid fronts stemming from southern part of the continent.

These factors give rise to several local climate aspects that are combined to the prevalent large scale features, consisting of semi-arid climate in the interior and a very humid regime along the coast (Nimer, 1989). The influence of local and global characteristics on the scaling properties of pluviometric records has been addressed in previous studies (Andrade et al., 1998; Miranda and Andrade, 1999; Miranda et al., 2004).

We base our investigation on two data sets ($S1$ and $S2$), one of them restricted to the state of Bahia, while the second includes data from stations located all over the Northeast region. The first one, provided by ADENE (Agência Nacional para o Desenvolvimento do Nordeste, Division of Bahia), contains daily precipitation records from 1979 to 2000, for 514 stations. The second one, collected by NCAR (National Center for Atmospheric Research, USA), contains daily precipitation records, from 1904 to 1983, for 2346 stations from all 9 states of NE Brazil, including Bahia. In Fig. 1, we show the geographical location of the stations in the data sets.

The stations of set $S1$, all of them located in the state of Bahia, are distributed over an irregular region bounded by a box of roughly 1000 km × 1000 km.The stations of the set $S2$ are distributed over a region of 2000 km × 1000 km, where the larger axis is directed along the south-north direction. To investigate the effect of latitude on our results, we have scrutinized the data in set $S2$ in three different ways. In first place, we take into account the stations to the north of ($S2$a) Northeast, what restricts the stations

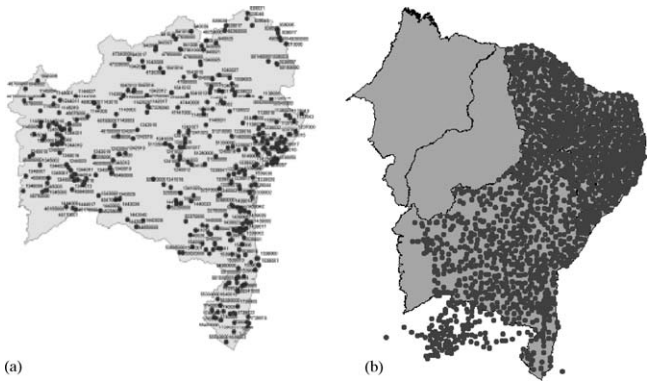

Fig. 1. Geographical distribution of stations in ADENE (a) and NCAR (b) data sets. The stations in states Piauí and Maranhão (northwest) were not included in the analysis.

to a region of roughly 1000 km × 1000 km. The stations of the second set ($S2b$) are distributed over roughly 1000 km × 1000 km square box, where the south-north axis includes some 500 km in the north part of the state of Bahia and 500 km in the south of the previous region. Finally, the third set takes into account all stations in the set $S2$.

We call to attention that, in both data sets, the number of stations with uninterrupted sequence of days with valid entries is rather small. So, in order to enrich statistics and minimize fluctuations, making the scaling behavior more visible, we consider the data from the time interval including the largest number of stations with valid entries. The time interval 1979–1983 results the best choice satisfying this condition for both $S1$ and $S2$.

3. Graph setup based on rainfall data

3.1. Basic concepts of graph theory

A graph $G(V,E)$ consists of a finite non-empty set $V(G)$ of elements v called vertices, a finite non-empty set $E(G)$ of elements e called edges, and a function $F(G)$ that associates to each element $e \in E(G)$, a pair $(v_1, v_2) \in V \times V$ called the extremes of e. Undirected graphs have an additional property ensuring that, if a pair (v_1, v_2) is associated with an edge $e_{12} \in E(G)$, the pair (v_2, v_1) is also included in $G(V,E)$. Graphs are usually represented by diagrams, where the elements of V and E correspond, respectively, to dots and lines connecting pairs of dots, in such a way that the above definition is satisfied.

A graph $G(E,V)$ of n vertices can be represented, in a very convenient way, by its adjacency matrix M. The matrix elements $m(i,j)$ of M are set to 1 or 0, according to whether the vertices i and j are connected by an edge or not. Therefore, two vertices i and j are adjacent, or neighbors, if $m(i,j) = 1$. The number k_i of adjacent vertices to a vertex $i \in V(G)$ is called the degree of i. The value k_i is obtained by summing over the elements $m(i,j)$ of the row i, as can be observed in Fig. 2.

The graph definition is very general, so that it can be used to describe many distinct physical situations. If we fix the number of nodes n, the resulting graph depends only on the rules that decide whether the pairs of nodes are connected by an edge. Such rules must be judiciously chosen if a graph is intended to represent a particular system. The resulting edge distribution may range from a completely ordered and regular pattern to a fully disordered one. For instance, the square lattice, defined on the surface of a two-dimensional torus, is a realization of a regular graph, where $k_i = 4$ for any i. By contrast, the one-parameter Erdös-Renyi graph, which is defined only by the constant probability $p < 1$ that any pair (i,j) is connected by an edge, is the paradigm of a fully random graph. If

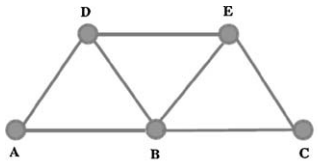

(a)

	A	B	C	D	E
A	0	1	0	1	0
B	1	0	1	1	1
C	0	1	0	0	1
D	1	1	0	0	1
E	0	1	1	1	0

(b)

Fig. 2. Example of a simple graph: (a) geometric representation where the nodes are labeled by capital letters running from A to E and (b) adjacency matrix, where lines and columns are labeled according to the nodes they correspond to.

$p = 1$, we obtain a complete ordered graph, in which all pairs of vertices are connected.

It is possible to assign a weight $w(i, j)$ to the edges of a graph. This is very useful when a graph is intended to describe a particular phenomenon, in which the strength of the interaction among the different degrees of freedom, represented by nodes, is non-uniform.

3.2. Pearson correlation criterion for graph construction

The methodology we use to define pluviometric graphs is based on the behavior of signal correlation. This approach has been previously used to build brain functional graphs (Eguiluz et al., 2005). In that work, the authors first divide the brain volume into geometrical cells that are associated with nodes. Next, the level of local brain activity, measured by different blood fluxes through distinct geometric cells in dynamical functional magnetic tomography, is recorded as function of time. In the current work, the geometrical brain cells are replaced by the meteorological stations, and the corresponding rainfall time records play the role of the local brain activity series. In addition to these basic ingredients, we also take into account the values $d(i,j)$ in our data set.

The essence of the method is to scrutinize the data, within a suitable time interval, and evaluate the cross-correlation function among individual time series. The presence of correlation is measured by linear correlation coefficients, as those proposed by Pearson, Spearman or Kendall (Kendall and Gibbons, 1990). For the current study, the Pearson coefficient $R(i,j)$ defined by

$$R(i,j) = \frac{n\sum_{t=1}^{n} S_{i,t}S_{j,t} - \sum_{t=1}^{n} S_{i,t}\sum_{t=1}^{n} S_{j,t}}{\sqrt{\left[n\sum_{t=1}^{n} S_{i,t}^2 - \left(\sum_{t=1}^{n} S_{i,t}\right)^2\right]\left[n\sum_{t=1}^{n} S_{j,t}^2 - \left(\sum_{t=1}^{n} S_{j,t}\right)^2\right]}} \quad (1)$$

is quite adequate to identify and characterize drought and rain periods. In (1), n represents the number of days in the considered time interval and $S_{x,t}$ represents the rain amount of station x on the tth day.

The set of Pearson coefficients $R(i,j)$, which can be regarded as matrix elements of a correlation matrix **R**, indicates how strongly correlated any pair of stations is. Adapting the method described previously (Eguiluz et al., 2005) **R** is used to define a graph, where the vertices consist of the stations in the data set, while the edges are inserted into the graph depending on the value of $R(i,j)$. Thus, by choosing a suitable threshold value R_{th}, the graph can be defined by its adjacency matrix as:

$$m(i,j) = \begin{cases} 1, & \text{if } R(i,j) \geq R_{th} \\ 0, & \text{if } R(i,j) < R_{th} \end{cases} \quad (2)$$

The existence of a common climate causality relation on two distinct stations is represented by the minimum level of correlation R_{th} required to add an edge to the graph. Within this procedure, it is not likely that fortuitous event coincidence, leading to weakly correlated events for a long enough time interval n, can be mixed with highly correlated events among those stations that depend on similar rain mechanisms. We have mainly adopted the same threshold value $R_{th} = 0.7$ used previously (Eguiluz et al., 2005), although we have explored also other values of R_{th}, as will be discussed in the next section.

The graphs generated according to (1) and (2) indicate how the rainfall correlation is spatially distributed. It is worthy calling the attention that locality is not necessarily the most important criterion for existence of edges in the graphs. Indeed, given two pairs of stations (i,j) and (k,l), we find many situations where $R(i,j) < R(k,l)$ but $d(i,j) < d(k,l)$.

This characteristic of **R** is adequate to capture several particularities in the spatial dependence of climate variables. As mentioned in Section 1, climate results from the coupling of local and global dynamics, as local topography and globally displacement of air masses. In such situations, small-scale heterogeneities may well coexist with large scale homogeneity.

In order to quantify the spatial dependence, we implemented a numeric algorithm to count $N(\varepsilon)$, the number of edges connecting pairs (i,j) of stations for which $d(i,j) \leq \varepsilon$. The algorithm runs until ε reaches the value corresponding to the largest distance between any two stations in the considered region. The dependence between $N(\varepsilon)$ and ε may indicate the existence of a fractal like scale invariant measure in that space. This is true if the resulting points in the $N(\varepsilon) \times \varepsilon$ plane follow a power law function

$$N(\varepsilon) \sim \varepsilon^{\alpha}. \quad (3)$$

The systematic analysis of graphs obtained for several time intervals and for distinct climatic regions of the world should reveal to which extent the scale invariance defined by (3) is a robust property of rainfall patterns. Furthermore, the obtained values of the exponent α, as well as the range of distances where (3) accurately fit the data, provide information on the local dependence of fractal-like properties of rain distribution. This may lead to the identification of one further useful fingerprint to characterize climatic diversity.

4. Spatial dependence of graphs

Let us first discuss the tests carried out to validate the algorithms and methodology used to obtain results for actual data. We start with the most simple situation, consisting of a square lattice with $23 \times 23 = 529$ nodes, where the distance between nearest neighbors is 31 km. For this particular choice, the number of nodes in the lattice and surface where they are distributed closely match the corresponding number of stations in the set $S1$ and area of the state of Bahia. We build a graph with connections between any pair of nodes and, for the purpose of reducing finite size effects, count the number $N(\varepsilon)$ of connected pairs of nodes only within a circle of radius ε centered at the point (356, 356) km. As expected, the slope α of the curve $\log(N(\varepsilon)) \times \log(\varepsilon)$ is nearly constant until $\varepsilon \sim 356$ km, as shown in Fig. 3. For larger values of ε, finite size effects (the circle diameter exceeds the side of the square) reduces the number $N(\varepsilon)$ in comparison to that for larger domains, so that the slope deviates from the value $\alpha = 2$ found for $\varepsilon \leq 356$ km.

Next, we considered complete graphs formed by 514 randomly distributed nodes into two two-dimensional domains: the same square box as before and the region limited by the actual border of the state of Bahia. Now $N(\varepsilon)$ includes all pairs (i,j) for which $d(i,j) \leq \varepsilon$. According to the curves shown in Fig. 3 we find, respectively, $\alpha = 1.92$ and 1.82 for random distributions on the square box and the region limited by the border of the state of Bahia.

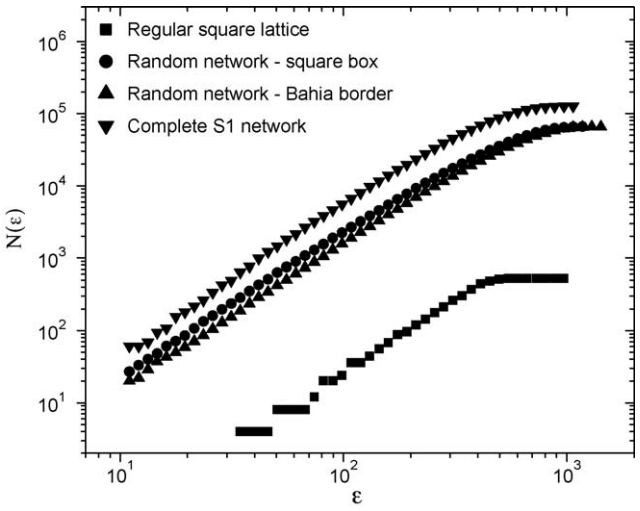

Fig. 3. Scaling analysis for complete graphs formed by the set of geographically disturbed stations and a regular lattice. Data refers to the number of connected pairs of nodes as function of the maximal edge size. Both sets show power law with exponent $\alpha \approx 2$.

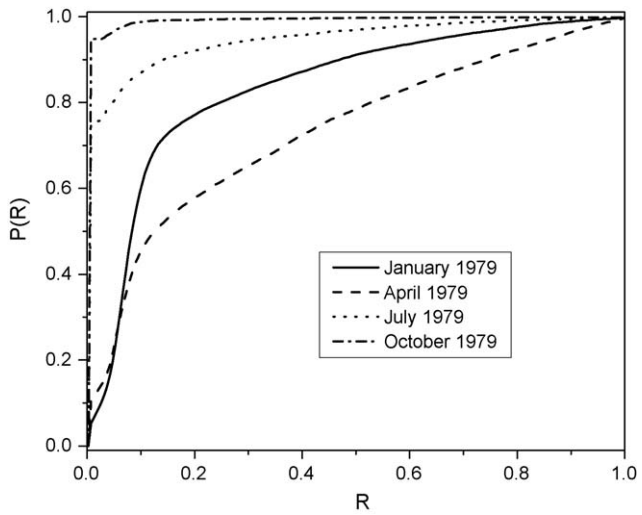

Fig. 4. Integrated distribution $P(R)$, as function of function of R for four distinct months in the year 1979. The rapid increase in the value of $P(R)$ for low values of R results from the pairs of low correlated stations. This contribution is greatly enhanced in the dryer months (October and July) in comparison to those with more abundant rainfall (April and January).

Finally, the last curve in Fig. 3 was obtained when we considered the complete graph formed by 514 nodes occupying the actual positions of the stations in the set $S1$. The scaling behavior with $\alpha = 1.93$ extends almost to $\varepsilon \leq 500$ km. A new feature is the presence of deviations from the power law behavior in the small scale region $\varepsilon < 20$ km. This behavior, which is also evident in the corresponding curve for the set $S2$, results from the decision not install pluviometric stations in two close places.

The complete graphs for the sets $S1$ and $S2$ correspond to those produced within the proposed framework when $R_{th} = 0$. At the other extreme value $R_{th} = 1$, the graphs consist only of isolated nodes, where α cannot be evaluated. Thus, the value of R_{th} plays an important role in the pattern of the obtained graphs. We present results mainly for $R_{th} = 0.7$, which is restrictive enough to explicit different graph patterns related to seasonality, and also lie far apart from the two extreme values 0 or 1 that carry no information on rainfall dynamics. As the results in Fig. 3 lead to values $\alpha \approx 2$, any decrease from this value results from changes in the graphs produced by precipitation dynamics.

To investigate the influence of the adopted value of R_{th}, let us consider the global correlation effect in our data set measured by Pearson coefficient. In Fig. 4, we draw $P(R)$, the integrated distribution of values of R for pairs of stations, as a function of R for the different analyzed regions and months of the year. The sharp increase in $P(R)$ for low values ($<R = 0.2$) results from an expressive number pairs of stations that are not significantly correlated. For all curves, it is verified that $P(R) > 0.7$ when $R > 0.5$, while they approach the normalized value $P = 1$ quite smoothly. Seasonal differences are indicated by a larger number of less correlated stations in the dry seasons, what is reflected in the height and the position of the step for $R < 0.2$. Despite these clear features, it is not possible to infer, from the bare analysis of $P(R)$, a precise value for the choice of an adequate value for R_{th}, apart from requiring that $P(R_{th})$ should be close to 1. As we show in Fig. 6b by direct comparison of results for different values of R_{th}, the conclusions we derive from results for the adopted value $R_{th} = 0.7$ are much the same to those for any value of R_{th} within a broad interval around it.

The results for the actual data fit well into the general framework we obtained for the test situations. Since our investigation covers the years 1979–1983, it required the construction and analysis of a total of $5 \times 12 \times 4$ distinct graphs of $N(\varepsilon) \times \varepsilon$ for the correlation measured over time interval of 1 month for each one of the four sets characterized in Section II.

The series of results in Fig. 5 evidence that pluviometric dynamics does affect the existence scaling behavior among Pearson-correlated set of stations. In contrast to the former situations (complete graph and regular lattice), where the results are only related to the geometrical/geographical distribution of stations, pluviometric dynamics influences the extension and strength of scaling. The new effect can still be observed because Pearson's methodology extends its range to larger scales, which clearly surpasses the limits indicated by the spatial Hurst exponent (~150 km). The main difference between the two measures is related to the fact that the former one accounts only for short-range causality relations in pluviometric phenomena.

In Fig. 5, we show a sample of the curves that lead to the evaluation of the exponents α. Each panel displays results for the January data in the subsequent years 1979–1983. In Fig. 5a and b, the horizontal axes indicate the presence of Pearson-correlated pairs of stations in the sets $S1$ and $S2a$ that are as distant as 800 km. Taking into account the aspects related to finite size effects of the samples, discussed for Fig. 3, we see that a power law is valid in the middle range scale (20–500 km). Similar graphs, obtained for the other months, lead to the corresponding values of α. The year averages of α, indicated by $\bar{\alpha}$, together with the year dispersion $\Delta\alpha$ (indicated by error bars), are drawn in Fig. 6 for the sets $S1$ and $S2a$. With the exception of the year 1980, when a particularly strong El-Niño effect globally influenced the world climate, the results indicate almost coincident values of $\bar{\alpha}$ for the two distinct sets. This indicates that, in each data set corresponding to the southern and northern parts of the region, the stations are Pearson-correlated in a very similar way.

These results can be compared with those derived from temporal and spatial Hurst analysis. They systematically indicate that the same series considered herein show a higher degree of persistence (large values of Hurst exponents H) in the lower latitude region $S2a$, expressed by a general trend in the value of H to decrease when the latitude increases $S1$. This has been explained by the presence of distinct driving rainfall systems in the northern and southern part of Northeast Brazil.

Before we discuss the results for the sets $S2b$ and $S2$, let us recall that they include stations from the two quoted sets $S1$ and $S2a$. The

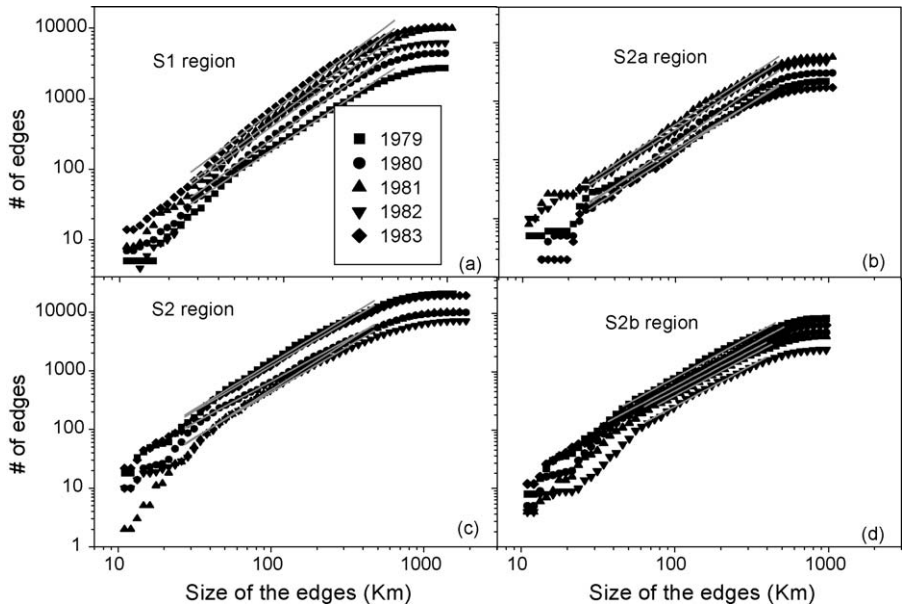

Fig. 5. Scaling analysis showing the same measure as in Fig. 3. Graphs were constructed based on Pearson coefficient values of January precipitation records of the January month for five successive years. Different regions in (a–d) are characterized in the main text. Gray straight lines indicate the regions where the slopes have been measured.

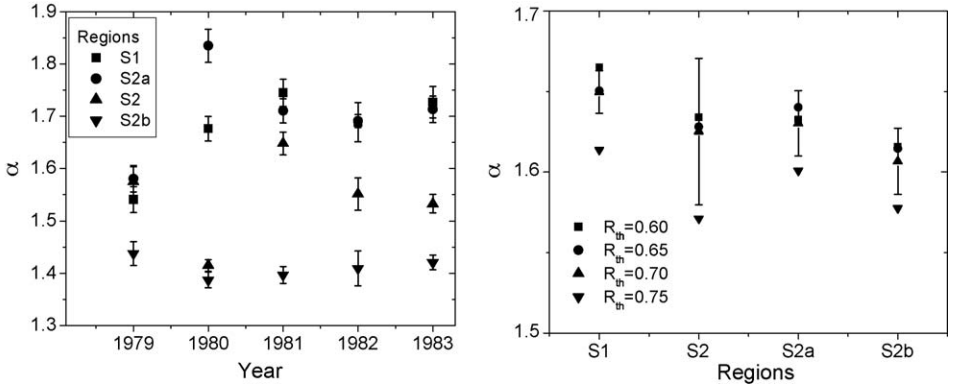

Fig. 6. (a) Year average values of α ($\bar{\alpha}$, symbols) and dispersion ($\Delta\alpha$—error bars) for the four different regions in Northeast Brazil. Regions driven mainly by the same pluviometric systems (*S*1 and *S*2*a*) are characterized by large values of $\bar{\alpha}$. Sets mixing stations coming from both *S*1 and *S*2*a* are characterized by small values of $\bar{\alpha}$. In general, $\bar{\alpha}$ seems to reflect homogeneity or heterogeneity of climatic influence in stations used to construct the graph. (b) Influence of the value of R_{th} on the values α for the different considered regions in a typical month (December 1982). Error bars correspond to the linear fit errors from the $R_{th} = 0.7$ data. When $R_{th} = 0.6$ and 0.65, the values of α are almost equal to those for $R_{th} = 0.7$. For $R_{th} = 0.75$ the values of α are comparatively lower, but the same conclusions regarding uniformity of rainfall regime within the analyzed set can be recovered.

scaling behavior for the January months are displayed in Fig. 5c and d, while average values $\bar{\alpha}$ and dispersion $\Delta\alpha$ are shown in Fig. 6. It is possible to observe that the scaling regions for the sets *S*2*b* and S2 are roughly the same as those for the sets *S*1 and *S*2*a*. Although the maximal distance between the stations of set *S*2 is twice as large as those of the other three sets, the scaling interval does not increase along the same way. The corresponding values of $\bar{\alpha} \in (1.39, 1.65)$ are characterized by a strong decrease in comparison to those of sets *S*1 and *S*2*a*, when $\bar{\alpha} \in (1.54, 1.85)$. The decrease is still more evident for the set *S*2*b*.

Despite the distinct persistent character of sets *S*1 and *S*2*a*, we note that they display similar values for $\bar{\alpha}$, which are larger than those for the sets *S*2*b* and S2. Since the later two sets include data from stations driven by distinct pluviometric systems, we conclude that the value of α is related to the uniformity of Pearson correlation within the considered region, not with persistence of the signal. This interpretation aggress with the stronger decrease observed for *S*2*b*, where the effect of mixing the influences of the distinct pluviometric systems is increased to a maximum.

5. Conclusions

In this work, we developed a new method that uncovers the existence of a new scale invariance property in pluviometric records within a given region. Despite the fact that the motivation of our work was provided by graph concepts, the specific results we presented herein could also be derived without reference to this mathematical theory. Our study is based on the construction of graphs among the pluviometric stations, whereby the presence of edges connecting pairs of stations depends on whether they are (are not) Pearson-correlated over a given time interval which, in the current study, was taken to be one month. As a general result, we find that this newly reported scale invariant property is present for all months and different sub-regions that have been investigated. Pairs of Pearson-correlated stations can be found even if the distance between them is very large. On the other hand, scaling behavior has been found in the length interval comprised between 20 and 500 km. The upper limit largely exceeds the bounds for scaling behavior in the spatial Hurst analysis. Thus, the

new method certainly identifies the presence of non-local couplings among pairs of quite distant stations, suggesting a new type of scale invariant behavior that has been overlooked by Hurst analysis.

The results for precipitation data in Northeast Brazil allow a clear interpretation of the new results. Indeed, the values for the scaling exponent α indicate that it assumes large values (>1.65) within regions that are subject to the same precipitation systems. In opposition to the analysis by temporal and spatial Hurst exponents, the current study does not distinguish, from the bare value of α, distinct patterns for the southern and northern regions of Northeast Brazil. However, the values of α for graphs that include stations of both sub-regions are noticeable smaller than the previous ones. This hints that small values of α indicate that the stations within the set suffer the influence of distinct climatic systems. Our results confirm the complex climate and precipitation patterns of Northeast Brazil.

The results we discussed above, based on a non-local causality paradigm, indicate that the development of this particular framework uncovers new aspects of the climate system. Several other properties from our analysis that are expressed by the measures used to characterize the obtained graphs will be discussed in a forthcoming work.

Acknowledgements

This work was partially supported by Brazilian agencies CNPq, FAPESB, CAPES. The data sets provided by ADENE and NCAR and all the contributions of the members and collaborators of the postgraduate program PPGM/UEFS are also acknowledged.

References

Andrade, R.F.S., Schellnhuber, H.J., Claussen, M., 1998. Analysis of rainfall records: possible relation to self-organized criticality. Physica A 254, 557–568.

Chaves, R.R., Cavalcanti, I.F.A., 2001. Atmospheric circulation features associated with rainfall variability over southern Northeast Brazil. Mon. Weather Rev. 129, 2614–2626.

Eguiluz, V.M., Chialvo, D., Cecchi, G.A., Baliki, M., Apkarian, A.V., 2005. Scale-free brain functional networks. Phys. Rev. Lett. 94, 018102.

Hastenrath, S., 1984. Predictability of north-east Brazil droughts. Nature 307 (February (9)), 531–533.

Hastenrath, S., Castro, L.C., Acietuno, P., 1987. The Southern oscillation in the tropical Atlantic sector. Contrib. Atmos. Phys. 60, 447–463.

Koscielny-Bunde, E., Bunde, A., Havlin, S., Roman, H.E., Goldreich, Y., Schellnhuber, H.-J., 1998. Indication of a universal persistence law governing atmospheric variability. Phys. Rev. Lett. 81, 729–732.

Kendall, M., Gibbons, J.D., 1990. Rank Correlation Methods, 5th ed. Oxford University Press, New York, 260pp.

Lovejoy, S., Mandelbrot, B., 1985. Fractal properties of rain and a fractal model. Tellus 37A, 209–232.

Lovejoy, S., Schertzer, D., 1991. Multifractal analysis techniques and the rain and cloud fields from 10^{-3} to 10^{6} m. In: Schertzer, D., Lovejoy, S. (Eds.), Scaling, Fractals and Non-linear Variability in Geophysics. Kluwer, pp. 111–144.

Mandelbrot, B.B., 1982. The Fractal Geometry of Nature. Freeman, San Francisco.

Mandelbrot, B.B., Wallis, J.R., 1969. Robustness of the rescaled range R/S in the measurement of noncyclic long-run statistical dependence. Water Resour. Res. 5, 967–988.

Miranda, J.G.V., Andrade, R.F.S., 1999. Rescaled range analysis of pluviometric records in northeast Brazil. Theor. Appl. Climatol. 63, 79–88.

Miranda, J.G.V., Andrade, R.F.S., da Silva, A.B., Ferreira, C.S., Gonzalez, A.P., Carrera López, J.L., 2004. Temporal and spatial persistence in rainfall records from Northeast Brazil and Galicia (Spain). Theor. Appl. Climatol. 77, 113–121.

Nimer, E., 1989. Climatologia do Brasil. Fundação Instituto Brasileiro de Geografia e Estatística, Rio de Janeiro (in Portuguese).

Rubalcaba, J.J.O., 1997. Fractal analysis of climatic data: annual precipitation records in Spain. Theoretical and Applied Climatology 56, 83–87.

Turcotte, D.L., 1992. Fractals and Chaos in Geology and Geophysics. Cambridge University Press, Cambridge, 221 pp.